Supporting information

Activating 2D nano-kaolinite via hybrid nanoparticles for enhanced phosphate capture

Yanfu Wei[1,+], Peng Yuan[1,2,+,], Dong Liu[1,2], Dusan Losic[3], Daoyong Tan[4], Fanrong Chen[1,2], Hongchang Liu[1], Junming Zhou[1,2], Peixin Du[1,2],Yaran Song[1,2]*

[1] CAS Key Laboratory of Mineralogy and Metallogeny/Guangdong Provincial Key Laboratory of Mineral Physics and Materials, Guangzhou Institute of Geochemistry, Chinese Academy of Sciences (CAS), Guangzhou 510640, China

[2] University of Chinese Academy of Sciences, Beijing 100049, China

[3] School of Chemical Engineering, The University of Adelaide, Adelaide, South Australia 5005, Australia

[4] Key Laboratory of Solid Waste Treatment and Resource Recycle, Ministry of Education, Southwest University of Science and Technology, Mianyang 621010, China

Email adress: yuanpeng@gig.ac.cn.

Experimental

Synthesis of LO-NKaol. In a typical procedure, a certain amount of NKaol prepared by mechanical milling for 24h[1], lanthanum hexahydrate, and glycine were separately added in a 10 mL test tube. The mass ratio of NKaol/La were set as 1/0.45. These mixtures were dissolved in deionized water followed by sonication for 30 min. The resulting suspension was placed in an oven and drying at 120°C for 2 hours to obtain a dried sample. The product was then calcinated in a tube furnace under 450°C for 2 hours. After cooling, the sample went through a 200-mesh sieve to obtain the final lanthanum oxycarbonate ($La_2O_2CO_3$, abbreviated as LO) nanoparticle-coated NKaol adsorbent (LO-NKaol) for phosphate removal. NKaol and NKaol calcinated at 450°C and 700°C as well as LO without NKaol (synthesized at the same condition of LO-NKaol) were used as control samples.

Phosphate adsorption. In the batch phosphate adsorption process, the 50 mg LO-NKaol and 20 mL of KH_2PO_4 were mixed in a 50-mL centrifuge tube and placed on a shaker (250 rpm and 25°C) for 1 d. For kinetic studies, the predetermined time intervals were set with a phosphate concentration of 300 mg P/L. Different concentrations of phosphate were used to evaluate the adsorption isotherms for phosphate on LO-NKaol, pristine NKaol, NKaol calcinated at 450°C and 700°C, and LO. The samples were shaken on a rotary shaker at 250 rpm and 25°C for 1 d. The pH of the solutions was maintained at 4.5 throughout the kinetic and isotherm adsorption.

After adsorption equilibrium, all samples were collected and centrifuged for 5 min at 8000 rpm for solid precipitate from the solution. The concentration of the phosphate in the solution was measured by the method of molybdenum-blue ascorbic acid and detected on a UV spectrophotometer at 580 nm. All tests were performed in triplicate. The adsorption performance, i.e., the quantity of phosphate adsorbed by per unit mass of the sample, Q_e (mg P/g), is calculated as using the following equation:

$$Q_e = (C_i - C_e)\, V / M \qquad (1)$$

in which Q_e represents the adsorbed amount of phosphate (mg P/g); C_i represents the initial concentration of phosphate (mg P/L); C_e represents the equilibrium concentration of phosphate (mg P/L); M represents the mass of the adsorbent (g); and V represents the volume of the solution (L).

The maximum adsorption capacity is the most important criteria, and high values of the maximum indicates efficient phosphate removal. We used the Langmuir model to fit the adsorption isotherm to get the maximum capacity for phosphate removal.

$$C_e / q_e = 1 / Q_m \cdot K_L + C_e / Q_m \qquad (2)$$

in which C_e (mg P/L) represents the equilibrium concentration of phosphate, and q_e (mg P/g) represents the corresponding adsorbed amount of phosphate; Q_m (mg P/g) represents the fitted maximum adsorption capacity, and K_L (L/mg) represents the Langmuir constant.

Characterization methods. Crystalline phases were characterized by X-ray powder diffraction patterns (XRD) using a Bruker D8 Advance diffractometer equipped with graphite monochromatized Cu Kα radiation (λ = 0.15406 nm); the samples included NKaol heated at 450°C, LO-NKaol and LO. The tube voltage is 40 kV with a tube current of 40 mA and a 1° 2θ/min scan rate from range of 3 to 50°. A Bruker Multimode 8 scanning probe microscope with a silicon tip on a nitride lever is used for atomic force microscopy measurements. ScanAsyst-air mode was used for scanning NKaol. To prepare the samples, a suspension of the powder (1.5 mg/ml) was prepared using de-ionized water (Millipore Inc.). 10–20 μm of this suspension is drop casted onto mica surface. After dried in air for 12h, the samples are rinsed with deionized water to remove nano-agglomerated clay particles from the mica substrate. The sample were dried in air for 1d before AFM measurement. Based on the AFM results, the thickness of Nkaol were measured and analyzed using Nano Measurer 1.2. The elemental contents (including elemental La content) in the LO-NKaol were measured by X-ray fluorescence spectrometer (XRF, Niton XL3t-800 X-ray fluorescence apparatus). The morphology and elemental content distribution of LO-NKaol and phosphate adsorbed LO-NKaol (P@LO-NKaol) samples were analyzed using Transmission electron microscopy (TEM) combined with energy-dispersive X-ray imaging (Titan Themis 200 TEM/EDX microscope) at 200 kV. For characterizing the cross-sectional surface of the NKaol particle, ultra-thin sections of NKaol were made. NKaol was embedded in epoxy resin which was allowed to harden, followed by cutting with an ultra-microtome. The ultra-thin sections of NKaol were further analyzed using TEM at 200 kV. The nitrogen N_2 adsorption-desorption test for NKaol and LO-NKaol were conducted via a Micromeritics ASAP-2000 nitrogen adsorption apparatus, and then the specific surface area and pore size distribution were analyzed accordingly. Fourier transform infrared (FTIR, a Bruker Vertex-70 FTIR spectrometer) was employed to detect the specific functional groups of the samples from 4000 to 400 cm^{-1} at room temperature by using dry potassium bromide for background subtraction. The interactions between LO and NKaol, LO-NKaol and phosphate were probed from X-ray photoelectron spectroscopy (XPS) using a Al Kα electron spectrometer from VG Scientific using 300W Al Kα radiation. Phosphorus K-edge XANES analyses of P@LO-NKaol were conducted on Beamline 4B7A at the Beijing Synchrotron Radiation Facility, China. The data were collected under fluorescence yield mode between −10 to +40 eV, relative to the P K-edge energy at 2151 eV using a step size of 0.2 eV between 2140 eV and 2190 eV. XANES spectra for each sample were baseline corrected and normalized using the ATHENA program under IFEFFIT interface[2,3]. The distribution of phosphate components among LO and Al_2O_3 in P@LO-

NKaol samples was determined by liner combination fitting (LCF) analyses over the relative energy range of −10 to +40 eV. The P@LO-NKaol sample used for XPS, FTIR, TEM, and XANES analysis were produced by mixing LO-NKaol with phosphate at 400 mg P/L for 1 d at pH of 4.5. Phosphate adsorbed on LO and Al_2O_3 (P@LO and P@ Al_2O_3) samples were produced by mixing Al_2O_3, and LO with phosphate solution at 1000 mg P/L and 600 mg P/L respectively for 1 d at pH of 4.5, used as references in LCF analysis.

Supporting figures

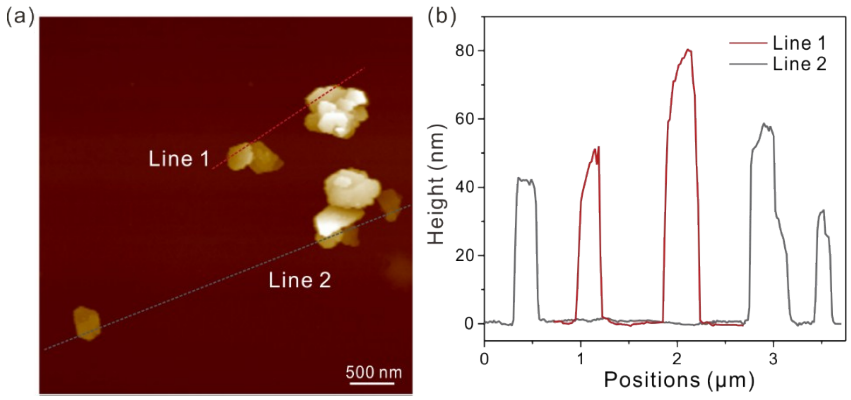

Figure S1 (a) AFM topography images of NKaol adsorbed on mica substrate, (b) the corresponding section analysis profiles (Line 1 and 2) showing the thickness distribution of NKaol nanoparticles.

The thickness (*c* dimension) of the NKaol is approximately 25-80 nm, indicating the 2D nano-structure of the kaolinite nanoclay. The *a-b* dimension of NKaol varies from tens to hundreds nanometers; and the morphology of the NKaol displays flat facets and a nanoplate-like, pseudo-hexagonal shape.

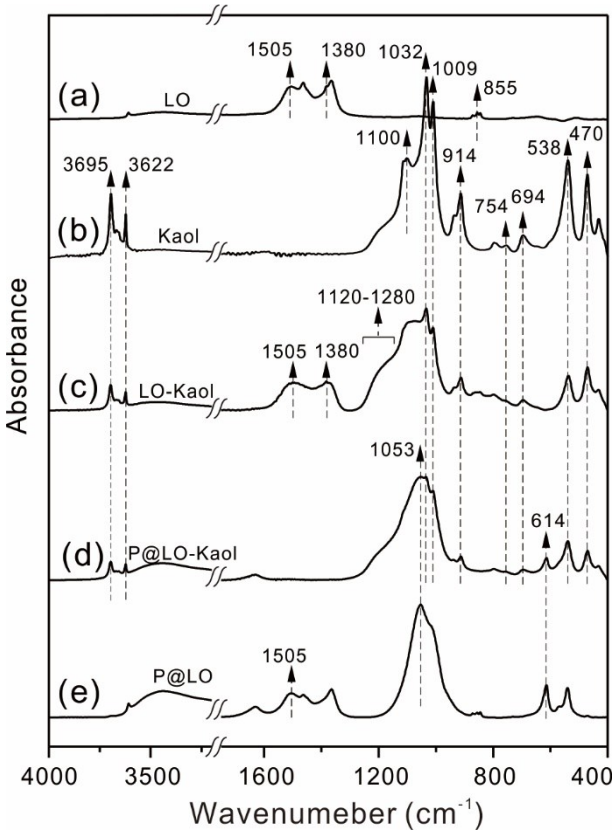

Figure S2 The FTIR spectra for (a) LO, (b) NKaol, (c) LO-NKaol, (d) phosphate adsorbed LO-NKaol (P@LO-NKaol), and (e) phosphate adsorbed LO (P@LO). The P@LO and P@LO-NKaol were prepared by mixing LO and NKaol with phosphate at concentrations of 700 and 1000 mg P/L, respectively; the pH was 4.5.

LO (Figure S2a) demonstrated typical vibrational bands at 1505, 1380 and 855 cm^{-1} corresponding to vibrations of CO_3^{2-} in LO.[4] Compared with pristine NKaol (Figure S2b), the LO-NKaol (Figure S2c) has an increased intensity of the band at 1120 to 1280 cm^{-1} and a new vibrational bands at 1505 and 1380 cm^{-1} demonstrating the occurrence of an Si−O−La bond[5] and CO_3^{2-} vibrations in LO-NKaol.

After phosphate adsorption saturation, the FTIR of P@LO (Figure S2e) shows the bands at 614 and 1053 cm^{-1} corresponding to the O−P−O bending and the P−O stretching vibration respectively[6]. These bending in FTIR of P@LO-NKaol overlap with the Si−O−Si vibration at 1100, 1032 and 1009 cm^{-1} in NKaol, along with the disappearance of vibrations of CO_3^{2-}. These results demonstrate the CO_3^{2-} groups between $(La_2O_2^{2+})_n$ layers of LO were almost complete replaced by $H_2PO_4^-$, which is the mainly phosphate species at pH 4.5[7]. However, the intensities of the CO_3^{2-} vibrations decreased only slightly in the spectrum of P@LO (Figure S2e). These results demonstrate the CO_3^{2-}−$H_2PO_4^-$ exchange ratio in LO is low, because the pure phase of aggregated LO nanoparticles limit LO exposure to phosphate (TEM in Figure S4). Thus, there is inefficient CO_3^{2-} for phosphate exchange; however, the well dispersed LO nanoparticles at surface of the NKaol help to exchange.

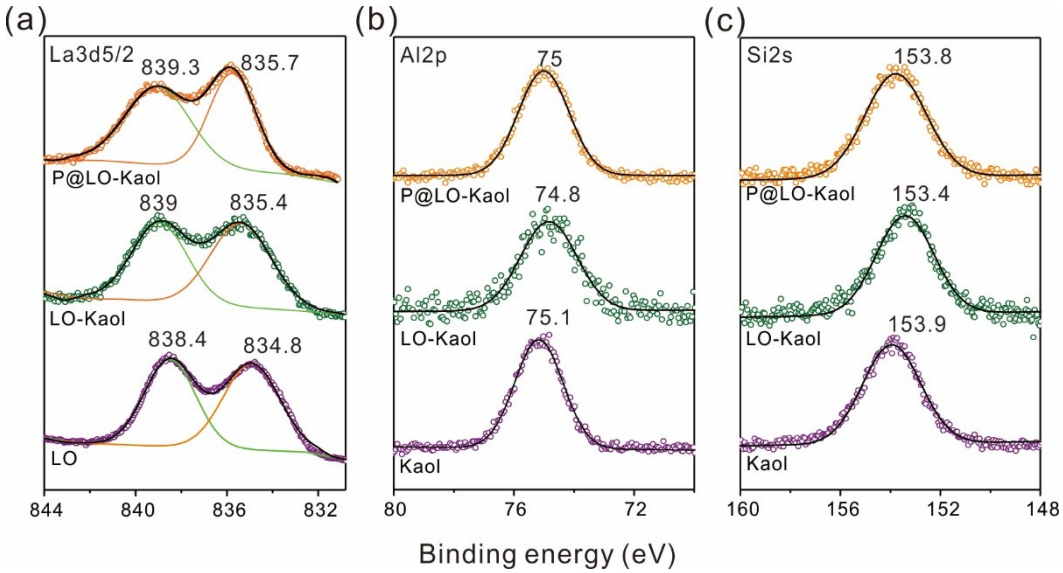

Figure S3 (a) XPS spectra of La3d5/2 for P@LO-NKaol, LO-NKaol and LO. (b) High-resolution XPS spectra of Si2s in NKaol, LO-NKaol and P@LO-NKaol, (c) High-resolution XPS spectra of Al2p in NKaol, LO-NKaol and P@LO-NKaol. The circles and solid lines is the measured and fitted XPS spectra respectively, and the value of the peaks are binding energies of La, Al and Si.

XPS data further confirms coating of LO at the surface of the NKaol. As shown in the high-resolution La 3d5/2 XPS spectrum of pure LO (Figure S3a), the characteristic band at 834.8 and 838.4 eV belongs to representative peaks of La 3d5/2. However, the binding energies of the La 3d5/2 in the spectrum of LO-NKaol shifted to higher value energies (835.4 and 839 eV) showing the interaction between of the coated LO and Al and Si in NKaol surface. This is accompanied by the shift of Al2p in NKaol (from 75.1 to 74.8 eV) (Figure S3b) and Si 2s in Karol (from 153.9 to 153.4 eV) (Figure S3c). These results reveal the formation of chemical bonds Si−O−La and Al−O−La for the La-NKaol.

XPS analysis of P@LO-NKaol further revealed the mechanism of surface complexation. The peak of La 3d5/2 for LO-NKaol after adsorption saturation is shifted to higher binding energies (at approximately 835.7 and 839.3 eV, Figure S3a), compared with the as-synthesized LO-Kao, indicating the formation of a La-O-P bond at the surface of the LO in LO-NKaol. Meanwhile, the binding energy of Al 2p (centered at 74.9 eV) of LO-NKaol (Figure S3b) shifts to 75.6 eV in P@LO-NKaol, revealing interactions between Al and P by forming an Al-O-P bond, which likely occurred at the Al-containing surface of NKaol. These results are consistent with the shifts corresponding to the related interactions in previous studies[8,9]. However, the Si 2s spectra of LO-NKaol after phosphate adsorption saturation does not show obvious changes compared with LO-NKaol (Figure S3c). This reveals the elemental Si in LO-NKaol is inactive for adsorbing phosphate.

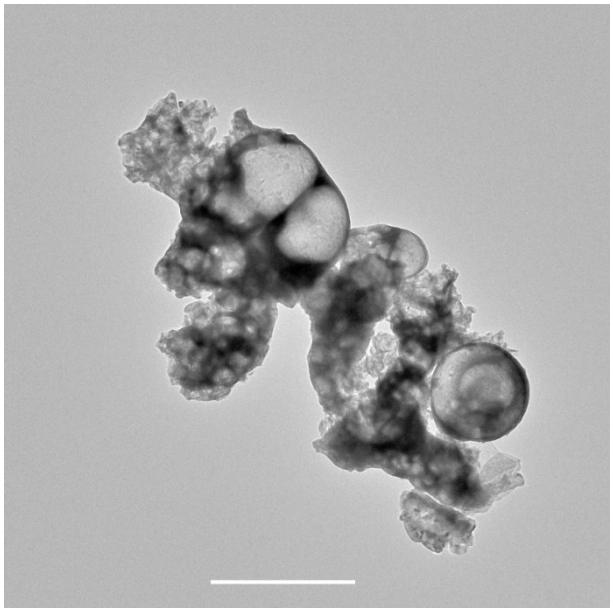

Figure S4. TEM images of aggregated LO nanoparticles, scale bars: 500μm.

Supporting tables

Table S1. XRF result of LO-NKaol shown in mass ratio and molar fraction.

Composition	Mass fraction (%)	Mole fraction (%)
Al	14.30	13.63
Si	15.80	14.46
O	39.41	63.33
La	28.24	5.22
C	1.22	2.60
Fe	0.38	0.17
Ca	0.20	0.02
Mg	0.23	0.25
K	0.08	0.05
Na	0.13	0.15

Table S2. The maximum phosphate adsorption capacity (Q_m) of adsorbents reported in the literature.

Materials	Q_m (mg P/g)	Refs.
La(III)-chelex resin	2.9	[10]
zirconium phosphate	8.28	[11]
La-lignocellulose	10.8	[12]
La-orange waste	13.9	[13]
La(III)-bentonite	14	[14]
La-mesoporous silicates	22	[15]
La-mesoporous SiO_2	23.1	[16]
humic acid coated magnetite	28.9	[17]
La/Fe-activated carbon fiber	29.4	[18]
La-porous carbon	32.4	[19]
La-$CuFe_2O_4$	32.6	[20]
lanthanum-decorated magnetite	44.8	[21]
La-biochar	46.4	[22]
La_2O_3	47.0	[23]
La-linked polystyrene	57.4	[24]
La(III) (hydr)oxides modified wheat straw	67.1	[25]
La/Al-Hydroxide Composite	71.6	[26]
La-zeolite	71.9	[27]
Fe-La-porous silica	72.0	[28]
La-silica foams	70.4	[29]
$La(OH)_3$-activated carbon fiber	16.1	[30]
Lanthanum-mesoporous silica	42.8	[31]
La-SBA	45.6	[32]
La-silica spheres	47.9	[33]
La-carbon nanotube	48.0	[34]
La-mesoporous ilicates	54.3	[35]
La-zeolites	58.2	[36]
Mesoporous α-Fe_2O_3	5.7	[37]
ZrO_2-Fe_3O_4	16.0	[38]
Zr-aminated wheat straw	24.8	[39]

Al-SBA	26.7	[9]
Ferrihydrite-diatomite	37.3	[40]
Fe-EDA-silica	43.3	[41]
ZrO_2-SiO_2 nanofiber	43.8	[42]
$MgCl_2$-alginate coated biochar	46.56	[43]
Zr(IV)-chitosan/Bentonite Composite	65.35	[44]
Fe_3O_4@ZrO_2 nanoparticle	69.44	[45]
Fe_3O_4@SiO_2-CeO	64.07	[46]
Mg/$La(OH)_3$	52.7	[47]
Crawfish char	70.9	[48]
Zr-MgFe-LDH(CO_3)	77	[49]
Mg-Al-LDH	47.3	[50]
Zr-graphite oxide	18.66	[51]
LO-NKaol	80	The present study

Table S3. Langmuir parameters fitted for adsorption isotherm of LO, NKaol, LO-NKaol, and NKaol calcinated at 450°C and 700°C, respectively.

Sample	K_L	Q_m	R^2
NKaol	2.271	0.1(mg P/g)	96.05
LO	0.003	173.2(mg P/g La)	98.85
LO-NKaol	0.056	286.3(mg P/g La)	99.99
NKaol 450°C	12.19	1.0(mg P/g)	99.74
NKaol 700°C	0.619	0.5(mg P/g)	96.41

Supporting References

1 M. S. Muhd Norhasri, M. S. Hamidah, A. M. Fadzil, A. G. Abd Halim and M. R. Zaidi, Advanced Materials Research, 2014, **925**, 28–32.
2 B. Ravel and M. Newville, *J. Synchrotron Radiat.*, 2005, **12**, 537–541.
3 M. Newville, *J. Synchrotron Radiat.*, 2001, **8**, 322–4.
4 L. M. Cornaglia, J. Múnera, S. Irusta and E. A. Lombardo, *Appl. Catal. Gen.*, 2004, **263**, 91–101.
5 N. Liu, Z. Wu, M. Li, S. Li, Z. Luo, Y. Li, L. Pan and Y. Liu, *ChemCatChem*, 2017, **9**, 1641–1647.
6 N. Y. Mostafa, H. M. Hassan and O. H. A. Elkader, *J. Am. Ceram. Soc.*, 2011, **94**, 1584–1590.
7 S. Dong, Y. Wang, Y. Zhao, X. Zhou and H. Zheng, *Water Res.*, 2017, **126**, 433–441.
8 L. Fang, Q. Shi, J. Nguyen, B. Wu, Z. Wang and I. M. C. Lo, *Environ. Sci. Technol.*, 2017, **51**, 12377–12384.
9 E. W. Shin, J. S. Han, M. Jang, S.-H. Min, J. K. Park and R. M. Rowell, *Environ. Sci. Technol.*, 2004, **38**, 912–917.
10 R. S. S. Wu, K. H. Lam, J. M. N. Lee and T. C. Lau, *Chemosphere*, 2007, **69**, 289–294.
11 Q. Zhang, Q. Du, T. Jiao, B. Pan, Z. Zhang, Q. Sun, S. Wang, T. Wang and F. Gao, *Chem. Eng. J.*, 2013, **221**, 315–321.
12 E. W. Shin, K. G. Karthikeyan and M. A. Tshabalala, *Environ. Sci. Technol.*, 2005, **39**, 6273–6279.
13 B. K. Biswas, K. Inoue, K. N. Ghimire, S. Ohta, H. Harada, K. Ohto and H. Kawakita, *J. Colloid Interface Sci.*, 2007, **312**, 214–223.
14 V. Kuroki, G. E. Bosco, P. S. Fadini, A. A. Mozeto, A. R. Cestari and W. A. Carvalho, *J. Hazard. Mater.*, 2014, **274**, 124–131.
15 J. Zhang, Z. Shen, W. Shan, Z. Chen, Z. Mei, Y. Lei and W. Wang, *J. Environ. Sci.*, 2010, **22**, 507–511.
16 E. Ou, J. Zhou, S. Mao, J. Wang, F. Xia and L. Min, *Colloids Surf. Physicochem. Eng. Asp.*, 2007, **308**, 47–53.
17 M. Rashid, N. T. Price, M. Á. Gracia Pinilla and K. E. O'Shea, *Water Res.*, 2017, **123**, 353–360.
18 J. Liu, Q. Zhou, J. Chen, L. Zhang and N. Chang, *Chem. Eng. J.*, 2013, **215–216**, 859–867.
19 P. Koilraj and K. Sasaki, *Chem. Eng. J.*, 2017, **317**, 1059–1068.
20 W. Gu, X. Li, M. Xing, W. Fang and D. Wu, *Sci. Total Environ.*, 2018, **619–620**, 42–48.
21 H. Fu, Y. Yang, R. Zhu, J. Liu, M. Usman, Q. Chen and H. He, *J. Colloid Interface Sci.*, , DOI:10.1016/j.jcis.2018.07.025.
22 Z. H. Wang, D. K. Shen, F. Shen and T. Y. Li, *Chemosphere*, 2016, **150**, 1–7.
23 J. Xie, Y. Lin, C. Li, D. Wu and H. Kong, *Powder Technol.*, 2015, **269**, 351–357.
24 Y. Zhang, B. Pan, C. Shan and X. Gao, *Environ. Sci. Technol.*, 2016, **50**, 1447–1454.
25 H. Qiu, C. Liang, J. Yu, Q. Zhang, M. Song and F. Chen, *Chem. Eng. J.*, 2017, **315**, 345–354.
26 R. Xu, M. Zhang, R. J. G. Mortimer and G. Pan, *Environ. Sci. Technol.*, 2017, **51**, 3418–3425.
27 J. Xie, Z. Wang, D. Fang, C. Li and D. Wu, *J. Colloid Interface Sci.*, 2014, **423**, 13–19.
28 C. Wang, X. Zheng, F. Zhang, Y. Huang and J. Pan, *RSC Adv.*, 2016, **6**, 87808–87819.
29 J. Yang, P. Yuan, H.-Y. Chen, J. Zou, Z. Yuan and C. Yu, *J. Mater. Chem.*, 2012, **22**, 9983–9990.
30 L. Zhang, Q. Zhou, J. Liu, N. Chang, L. Wan and J. Chen, *Chem. Eng. J.*, 2012, **185–186**, 160–167.
31 W. Y. Huang, X. Yu, J. P. Tang, Y. Zhu, Y. M. Zhang and D. Li, *Microporous Mesoporous Mater.*, 2015, **217**, 225–232.
32 J. Yang, L. Zhou, L. Zhao, H. Zhang, J. Yin, G. Wei, K. Qian, Y. Wang and C. Yu, *J. Mater. Chem.*, 2011, **21**, 2489–2494.
33 W. Huang, Y. Zhu, J. Tang, X. Yu, X. Wang, D. Li and Y. Zhang, *J. Mater. Chem. A*, 2014, **2**, 8839–8848.
34 E. Zong, X. Liu, J. Wang, S. Yang, J. Jiang and S. Fu, *J. Mater. Sci.*, 2017, **52**, 7294–7310.
35 J. Zhang, Z. Shen, W. Shan, Z. Mei and W. Wang, *J. Hazard. Mater.*, 2011, **186**, 76–83.
36 J. Goscianska, M. Ptaszkowska-Koniarz, M. Frankowski, M. Franus, R. Panek and W. Franus, *J. Colloid Interface Sci.*, 2018, **513**, 72–81.

37 H. Liang, K. Liu and Y. Ni, *J. Taiwan Inst. Chem. Eng.*, 2017, **71**, 474–479.
38 L. Fang, B. Wu and I. M. C. Lo, *Chem. Eng. J.*, 2017, **319**, 258–267.
39 H. Qiu, C. Liang, X. Zhang, M. Chen, Y. Zhao, T. Tao, Z. Xu and G. Liu, *Acs Appl. Mater. Interfaces*, 2015, **7**, 20835–20844.
40 W. H. Xiong and J. Peng, *Water Res.*, 2008, **42**, 4869–4877.
41 W. Chouyyok, R. J. Wiacek, K. Pattamakomsan, T. Sangvanich, R. M. Grudzien, G. E. Fryxell and W. Yantasee, *Environ. Sci. Technol.*, 2010, **44**, 3073–3078.
42 X. Wang, L. Dou, Z. Li, L. Yang, J. Yu and B. Ding, *ACS Appl. Mater. Interfaces*, 2016, **8**, 34668–34676.
43 X. Cui, X. Dai, K. Y. Khan, T. Li, X. Yang and Z. He, *Bioresour. Technol.*, 2016, **218**, 1123–1132.
44 J. Wang, Y. Liu, P. Hu and R. Huang, *Environ. Prog. Sustain. Energy*, 2018, **37**, 267–275.
45 Z. Wang, M. Xing, W. Fang and D. Wu, *Appl. Surf. Sci.*, 2016, **366**, 67–77.
46 D. Hong, Z. Yanling, D. Qianlin, W. Junwen, Z. Kan, D. Guangyue, X. Xianmei and D. Chuanmin, *J. Rare Earths*, 2017, **35**, 984–994.
47 L. Fang, R. Liu, J. Li, C. Xu, L.-Z. Huang and D. Wang, *Water Res.*, 2018, **130**, 243–254.
48 J.-H. Park, J. J. Wang, R. Xiao, B. Zhou, R. D. Delaune and D.-C. Seo, *J. Colloid Interface Sci.*, 2018, **525**, 143–151.
49 R. Chitrakar, S. Tezuka, J. Hosokawa, Y. Makita, A. Sonoda, K. Ooi and T. Hirotsu, *J. Colloid Interface Sci.*, 2010, **349**, 314–320.
50 K. Kuzawa, Y.-J. Jung, Y. Kiso, T. Yamada, M. Nagai and T.-G. Lee, *Chemosphere*, 2006, **62**, 45–52.
51 E. Zong, D. Wei, H. Wan, S. Zheng, Z. Xu and D. Zhu, *Chem. Eng. J.*, 2013, **221**, 193–203.